

Supplementary Information

Nacre-inspired Integrated Nanocomposites with Fire Retardant Properties by Graphene Oxide and Montmorillonite

Peng Ming^{a†}, Zhaofei Song^{a†}, Shanshan Gong^{a†}, Yuanyuan Zhang^a, Jianli Duan^a, Qi Zhang^a, Lei Jiang^a and Qunfeng Cheng^{a, b*}

^aKey Laboratory of Bio-inspired Smart Interfacial Science and Technology of Ministry of Education, School of Chemistry and Environment, BeiHang University Beijing 100191, P. R. China

^bState Key Laboratory for Modification of Chemical Fibers and Polymer Materials, Donghua University, Shanghai 201620, P. R. China

E-mail: cheng@buaa.edu.cn

These three authors contributed equally to this work.

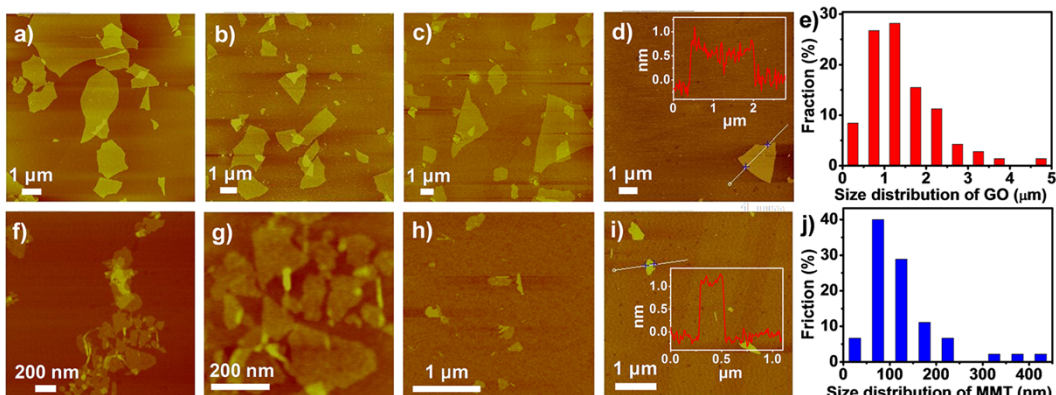


Figure S1. (a-d) AFM images of GO nanosheets deposited on mica plate. (e) Size distribution of GO nanosheets. The average diameter of GO nanosheets is about 1.2 μm , and the thickness is about 0.75 nm. (f-i) AFM images of MMT platelets deposited on mica plate. (j) Size distribution of MMT platelets. The average size is about 100 nm, and the thickness is about 1.2 nm.

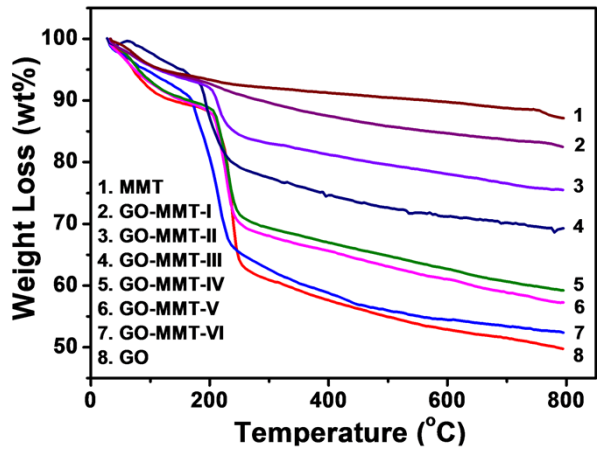


Figure S2. TGA curves of pure GO, MMT and different ratios of GO-MMT binary layered materials under N₂ with raising rate of temperature of 20°C/min.

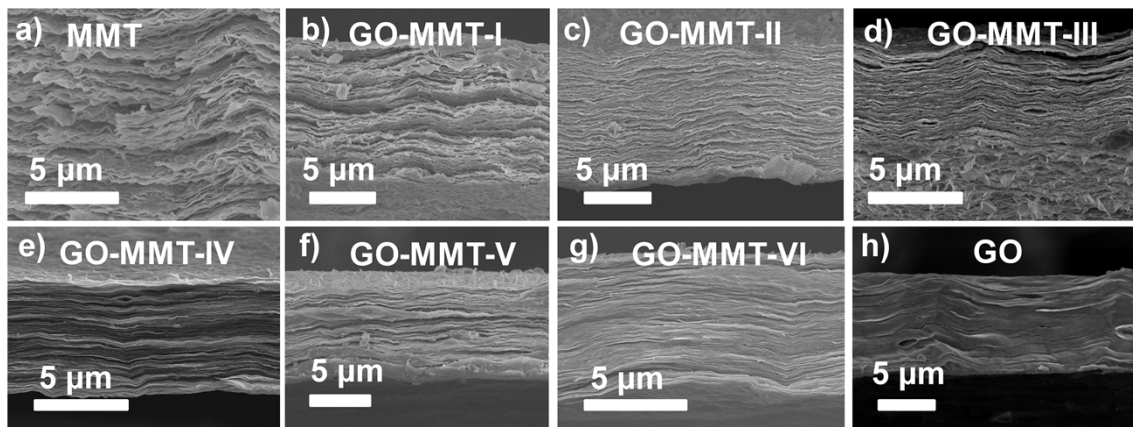


Figure S3. Cross-section morphology: (a) MMT, (b) GO-MMT-I, (c) GO-MMT-II, (d) GO-MMT-III, (e) GO-MMT-IV, (f) GO-MMT-V, (g) GO-MMT-VI, and (h) GO, respectively, which show typical nacre-like layered structure.

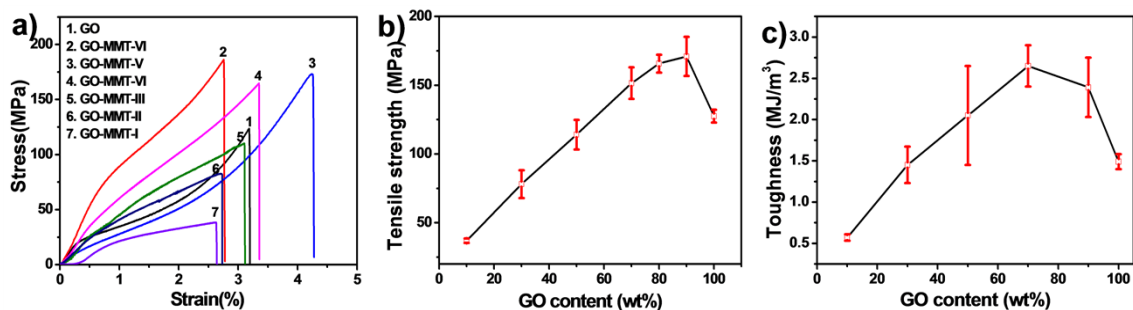


Figure S4. a) The typical stress-strain curves and mechanical properties of GO film and the GO-MMT binary hybrid layered materials with different GO contents.b) and c) The tensile strength and toughness of GO-MMT binary hybrid layered materials shows the maximum values when the ratio of GO to MMT is 90:10.

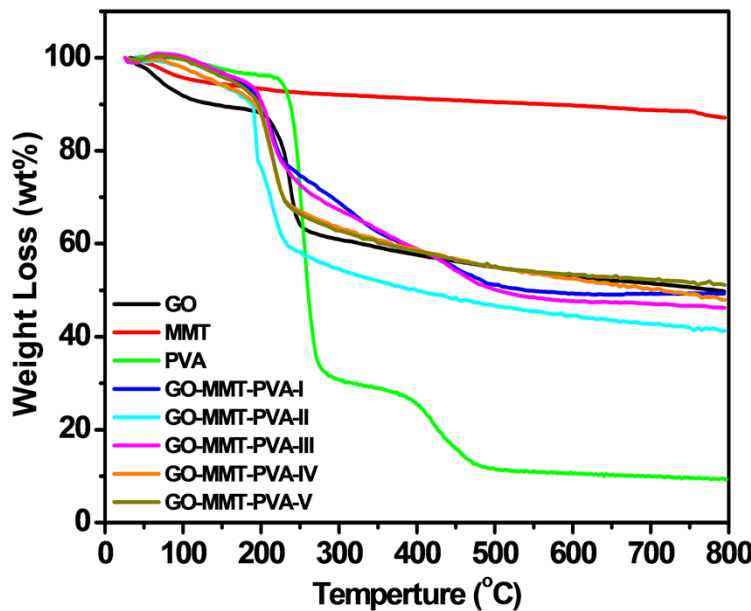


Figure S5. TGA curves of pure GO, MMT, PVA, GO-PVA,MMT-PVA and GO-MMT-PVA nanocomposites with different PVA content under N₂ with raising rate of temperature of 20°C/min.

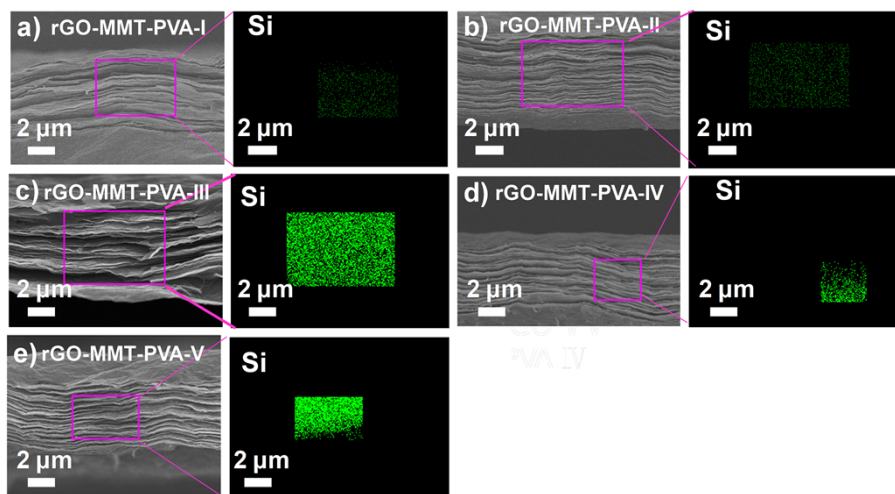


Figure S6. The cross-section morphology and EDS of the rGO-MMT-PVA ternary bioinspired nanocomposites: a) rGO-MMT-PVA-I, b) rGO-MMT-PVA-II, c) rGO-MMT-PVA-III, d) rGO-MMT-PVA-IV,e) rGO-MMT-PVA-V, respectively. EDS indicates the uniform distribution of Si element in the ternary bioinspired nanocomposites.

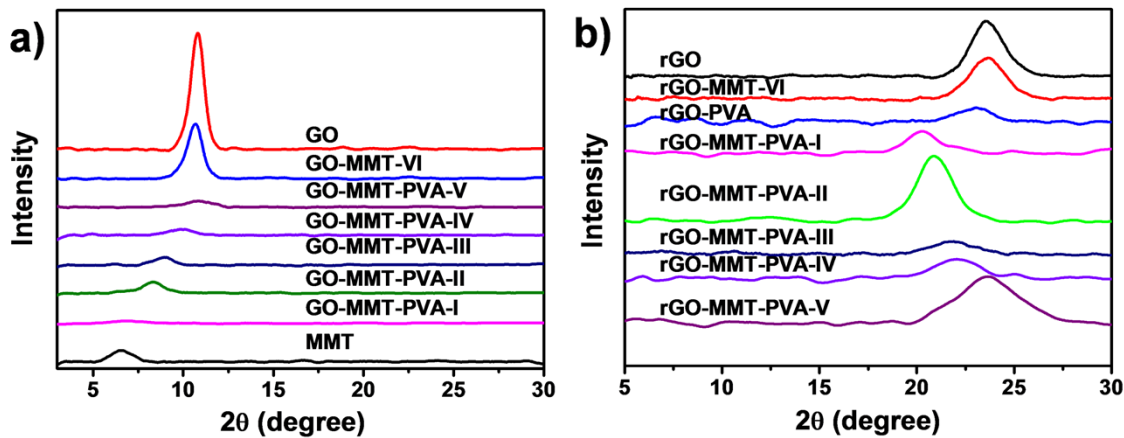


Figure S7. XRD curves of MMT, GO film, GO-MMT binary hybrid layered materials and GO-MMT-PVA ternary nanocomposites before (a) and after (b) HI reduction.

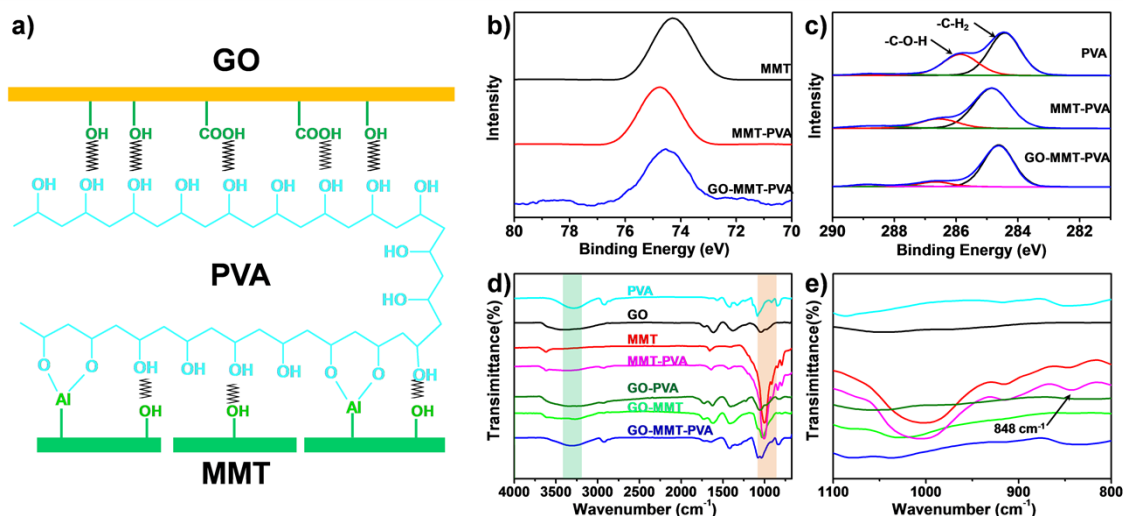


Figure S8. a) Schematic illustration of interface interactions between GO, PVA and MMT, including the hydrogen and covalent bondings. b) Al 2p orbital spectra for MMT and MMT-PVA, shows a positive energy shift, indicating the increased oxidation state of the Al. c) C 1s orbital spectra for PVA, MMT-PVA, and GO-MMT-PVA nanocomposites. XPS spectra were fitted in two major peaks at 284.4 eV and 285.9 eV correspond to $-\text{C}-\text{H}_2$ and $-\text{C}-\text{O}-\text{H}$ carbons, respectively. d) and e) FTIR spectra for PVA, GO, MMT, MMT-PVA, GO-PVA, GO-MMT and GO-MMT-PVA nanocomposites. The spectrum of MMT-PVA shows suppression of the C-O-H vibrations at peak of 3290 cm^{-1} due to the covalent bonding with the MMT. Arrow points the characteristic vibration peak of Al-O-C at 848 cm^{-1} , indicating the covalent bonding between PVA and MMT. These results are very well consistent with the previous report.¹⁷

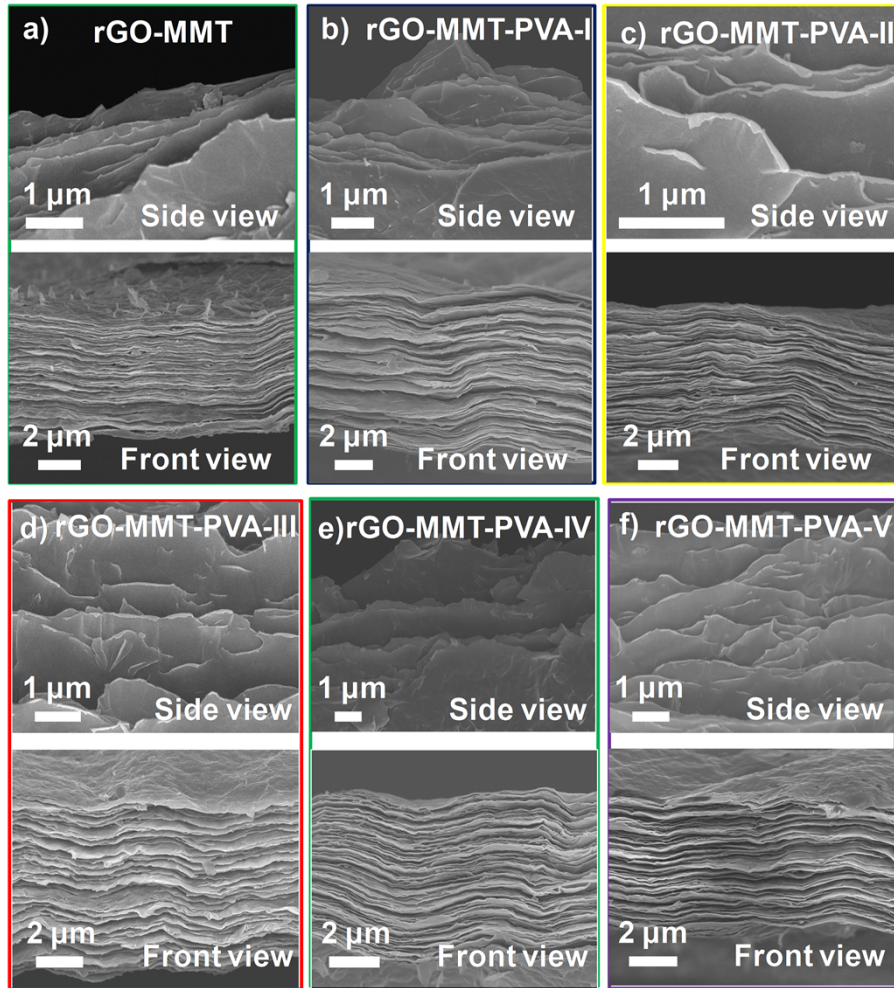


Figure S9. Fracture morphology of nanocomposites: a) rGO-MMT-VI , b) rGO-MMT-PVA-I, c) rGO-MMT-PVA-II, d) rGO-MMT-PVA-III, e) rGO-MMT-PVA-I V, and f) rGO-MMT-PVA-V, respectively.

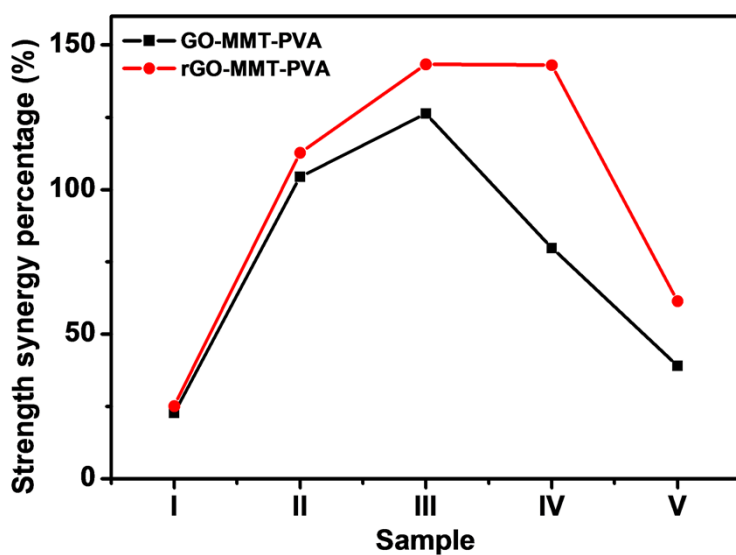


Figure S10. Synergy percentage (%) shows a maximum value in sample of ternary rGO-MMT-PVA-IV bioinspired nanocomposites.

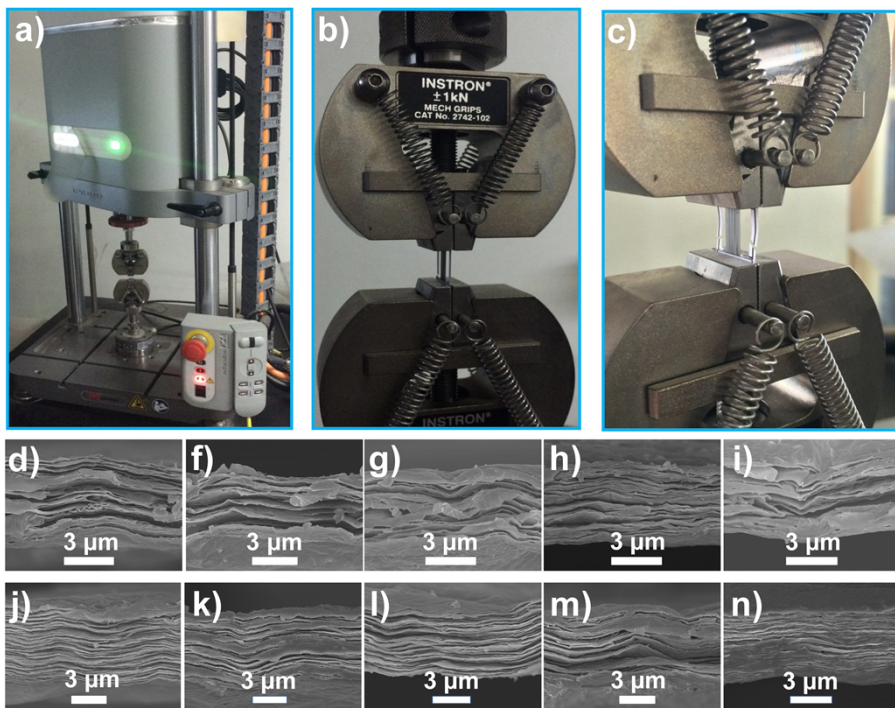


Figure S11. (a-c) The digital pictures of the fatigue testing in tension mode, (d-i) Fracture morphologies of binary rGO-MMT nanocomposites, which are corresponding to 6, 11, 405, 7407, 85532 cycles to Failure. (j-n) Fracture morphologies of ternary rGO-MMT-PVA nanocomposites, which are corresponding to 39, 122, 3360, 14091, 47005 cycles to Failure.

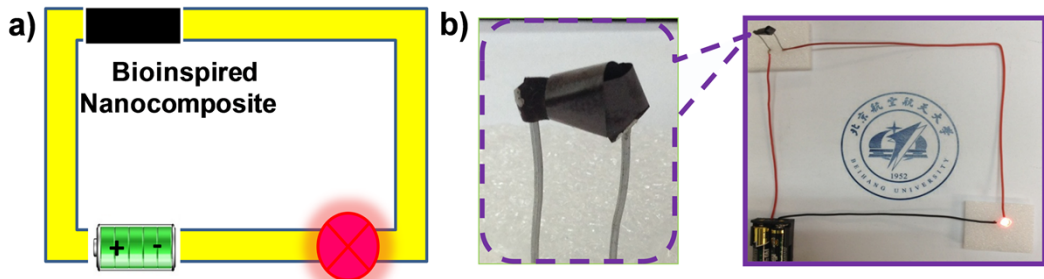


Figure S12. A LED red bulb was connected with the power supply, showing that the bioinspired nanocomposite cable functioned well for the entire testing period. (a) Schematics of the circuit of bioinspired nanocomposites. (b) The ternary rGO-MMT-PVA-IV bioinspired nanocomposites with a tie knot as a part of conductive media connected with power supply.

Table S1. GO content and the electrical conductivity of GO-MMT binary hybrid layered materials

Sample	Input GO Content (wt%)	GO content by TGA (wt%)	Electrical conductivity after HI reduction (S/cm)
GO	--	--	184.9±2.7
GO-MMT-I	10	12.3	5.3±0.1
GO-MMT-II	30	31.1	60.2±9.4
GO-MMT-III	50	47.5	138.5±6.5
GO-MMT-IV	70	77.3	149.0±8.0
GO-MMT-V	80	79.9	151.1±7.3
GO-MMT-VI	90	93.0	179.0±2.4

Table S2. The mechanical property of GO and GO-MMT binary hybrid layered materials with different GO contents

Sample	Tensile strength(MPa)	Toughness(MJ/m ³)
Pure GO	128.4 ± 11.3	2.4 ± 0.2
Reduced GO	178.1 ± 3.2	3.3 ± 0.3
GO-MMT-I	36.9 ± 1.6	0.6 ± 0.1
GO-MMT-II	78.1 ± 10.1	1.5 ± 0.2
GO-MMT-III	114.0 ± 10.7	2.1 ± 0.6
GO-MMT-IV	151.5 ± 11.6	2.7 ± 0.3
GO-MMT-V	165.7 ± 6.5	2.9 ± 0.2
GO-MMT-VI	171.0 ± 14.2	2.7 ± 0.3

Table S3. PVA content and the electrical conductivity of rGO-MMT-PVA ternary bioninspired nanocomposites

Sample	Input PVA content (wt%)	PVA content by TGA (wt%)	Electrical conductivity after HI reduction (S/cm)
GO-MMT-PVA-I	50	43.8	3.5 ± 0.2
GO-MMT-PVA-II	25	23.6	21.1 ± 5.2
GO-MMT-PVA-III	15	13.0	68.1 ± 5.3
GO-MMT-PVA-IV	10	9.4	130.0 ± 9.1
GO-MMT-PVA-V	5	2.6	136.4 ± 5.5

Table S4. The d-spacing of the GO film and the GO-MMT hybrid layered materials and GO-MMT-PVA ternary nanocomposites before and after HI reduction

Sample	d-spacing (nm)	
	Before HI reduction	After HI reduction
GO	0.82	0.37
GO-MMT (90:10)	0.84	0.38
GO-MMT-PVA-I	1.43	0.44
GO-MMT-PVA-II	1.06	0.42
GO-MMT-PVA-III	0.97	0.41
GO-MMT-PVA-IV	0.88	0.39
GO-MMT-PVA-V	0.83	0.38

Table S5. Mechanical properties of MMT-PVA, GO-PVA, GO-MMT-PVA, and rGO-MMT-PVA nanocomposites; and their calculated synergy percentage.

Sample	Strength (MPa)	Toughness (MJ/m ³)	Strength synergy percentage (%)
MMT-PVA	172.5 ± 9.3	1.8 ± 0.1	-
GO-PVA	167.1 ± 12.3	1.1 ± 0.3	-
rGO-PVA	274.4 ± 22.6	5.1 ± 0.2	-
GO-MMT-PVA-I	179.8 ± 34.1	1.4 ± 0.5	22.8
rGO-MMT-PVA-I	183.3 ± 7.6	5.8 ± 0.8	25.2
GO-MMT-PVA-II	299.4 ± 10.5	4.4 ± 1.0	104.4
rGO-MMT-PVA-II	311.6 ± 13.5	5.8 ± 0.4	112.8
GO-MMT-PVA-III	331.4 ± 17.6	4.9 ± 0.9	126.3
rGO-MMT-PVA-III	356.3 ± 23.7	5.3 ± 0.1	143.3
GO-MMT-PVA-IV	263.3 ± 28.7	7.4 ± 0.2	79.9
rGO-MMT-PVA-IV	356.0 ± 15.5	7.5 ± 1.1	143.1
GO-MMT-PVA-V	203.6 ± 5.9	6.4 ± 0.5	39.1
rGO-MMT-PVA-V	236.4 ± 19.8	6.9 ± 0.9	61.4

Table S6. The detailed mechanical properties of our ternary bioinspired nanocomposites, natural nacre and other GO-based layered materials

Layered Materials	Strength (MPa)	Toughness (MJ/m ³)	Reference
Nacre	200	2.6	[4]
GO-PMMA	148.3	2.35	[28]
rGO-PVA	188.9	2.52	[29]
rGO-SL	300	2.8	[30]
GO-Ca ²⁺	125.8	0.31	[31]
GO-Mg ²⁺	80.6	0.13	[31]
GO-Fe ³⁺	169.3	0.42	[32]
GO-GA	101	0.3	[23]
GO-PAA	91.9	0.15	[24]
GO-Borate	185	0.14	[25]
PGO-PEI	209.9	0.23	[26]
rGO-PCDO	129.6	3.91	[27]
rGO-PDA	204.9	4.4	[20]
rGO-MoS ₂ -TPU	235.3	6.9	[7]
rGO-MMT-PVA	356.0	7.5	[This work]